INTERNATIONAL JOURNAL OF ADVANCED STRUCTURAL ENGINEERING (2025) 15

Comprehensive Flexural Analysis of High-Performance Fiber-Reinforced Concrete Based on Mix Design and Energy/Post-Peak Strength Indices

Peyman FarhadiYeganeh[1], Maryam Firoozi Nezamabadi[1], Ata Hojatkashani[1]*, Abbas Akbarpour NikghalbRashti[1], Hassan Abbasi[1]

[1]Department of Civil Engineering, ST.C., Islamic Azad University, Tehran, Iran

*Corresponding Author: a_hojatkashani@iau.ac.ir

Abstract:

This study experimentally investigates the flexural behavior of high-performance fiber-reinforced cementitious composites (HPFRCCs) incorporating polypropylene fibers, with a particular focus on the influence of mix design parameters. Forty-four mixtures with varying proportions of cement, metakaolin, silica fume, slag, and limestone powder were tested under three-point bending conditions. The load–displacement responses were analyzed to extract a set of energy-based ductility and toughness indicators that characterize the post-cracking performance of the composites. The results revealed that ductility and residual load capacity were highly dependent on binder composition, especially the balance between cement, metakaolin, and slag contents. Correlation analysis using Spearman's rank coefficients showed that higher cement and metakaolin levels improved post-peak stability and energy dissipation, whereas excessive slag content led to greater softening and reduced toughness. These findings highlight that optimal mechanical performance in HPFRCCs arises not merely from strength maximization, but from a well-optimized mix design that enhances both energy absorption and post-cracking stability critical attributes for durable and seismic-resistant structures.

Keywords: HPFRCC, load–displacement curve, ductility indices, toughness, polypropylene fibers, Spearman correlation,mix design.

Highlights

- This study introduces a new method to evaluate flexural behavior by using energy-based measures that give a clearer view of post-cracking performance.
- The findings show that balanced material composition greatly improves stability after cracking and increases the ability to absorb energy.
- The work presents a fresh analytical approach that helps identify mix designs with better toughness and more reliable post-cracking behavior.

1. Introduction

The mechanical performance of High-Performance Fiber-Reinforced Cementitious Composites (HPFRCCs) under flexural loading is fundamentally governed by their post-cracking behavior, which distinguishes them from conventional concrete through the capacity to sustain load beyond first cracking via fiber-bridging mechanisms[1,2]. Unlike brittle failure in ordinary concrete, HPFRCCs often exhibit strain-hardening characteristics, manifested as a distinct ascending or plateau region in the post-peak segment of the load–displacement (P–Δ) curve obtained from standardized flexural tests. This behavior is critical in structural applications subjected to dynamic or seismic actions, where energy dissipation, deformation capacity, and residual load-carrying ability directly influence structural safety and collapse prevention[3,4]. Consequently, the accurate characterization of post-cracking response through quantitative metrics derived from P–Δ curves has become a central focus in the development and evaluation of advanced cementitious composites[5].

A comprehensive assessment of flexural performance necessitates moving beyond conventional strength-based parameters toward energy- and deformation-based indices that capture the full spectrum of material behavior from elastic response through crack initiation, peak load, softening, and residual capacity[6]. In this context, several ductility and toughness indices have been proposed in the literature to extract meaningful mechanical insights from experimental P–Δ data[7]. Notable among these are the energy-based ductility index (μ_E), which quantifies the ratio of post-peak to elastic energy absorption; the softening ductility ratio (SDR), defined as the residual load at a specified displacement normalized by the peak load; the residual toughness factor (RTF), representing the proportion of total energy dissipated after peak load; and the toughness modulus (TM), which normalizes total absorbed energy by specimen volume to enable geometry independent comparisons[8,9]. These indices collectively provide a multidimensional perspective on material performance, reflecting not only strength but also deformation tolerance, crack stability, and fiber efficiency in stress transfer across cracks[7,10].

The shape and characteristics of the P–Δ curve and by extension, the values of these derived indices are highly sensitive to mixture composition, particularly the type and dosage of supplementary cementitious materials (SCMs) and fibers[11]. Polypropylene (PP) fibers, widely used due to their cost-effectiveness, chemical resistance, and ease of dispersion, contribute significantly to post-cracking ductility through pull-out and bridging mechanisms[12,13]. However, their effectiveness is strongly modulated by the properties of the cementitious matrix, which in turn depend on the nature and proportions of SCMs such as metakaolin (MTK), silica fume (SF), ground granulated blast-furnace slag (SL), and limestone powder (LP)[14]. Metakaolin, for instance, enhances matrix density and interfacial bond strength through its high pozzolanic reactivity, potentially improving fiber–matrix interaction and post-peak load recovery. Silica fume refines pore structure and increases early-age strength but may reduce workability if not properly balanced. Limestone powder primarily acts as a filler that improves particle packing and hydration kinetics, though excessive replacement of cement can induce a dilution effect, weakening the matrix. Slag contributes to long-term durability but may alter rheology and delay strength development, indirectly affecting fiber dispersion and bonding Despite extensive research on fiber-reinforced concretes, a systematic experimental investigation linking the quantitative features of P–Δ curves specifically the suite of energy-based ductility and toughness indices to the precise compositional variables in HPFRCCs containing polypropylene fibers remains limited[15,16]. Many existing studies focus on qualitative descriptions of load–deflection responses or rely on a single performance metric (e.g., flexural strength or first-crack deflection), thereby overlooking the complex interplay between multiple post-cracking characteristics[17]. Several studies have investigated the flexural behavior and toughness of concrete reinforced with polypropylene fibers (PP). For instance, Smarzewski compared the effects of PP and basalt fibers in self-compacting concrete (SCC), evaluating flexural toughness based on the area under the load–deflection curve. However, this study primarily focused on fiber type and did not examine the influence of binder composition or multiple post-cracking energy indices[18]. Similarly, Wei et al. reported that incorporating PP fibers in reinforced concrete beams enhances crack control and deformation capacity, although their work is limited to reinforced systems and does not address the role of supplementary cementitious materials (SCMs)[19]. In another investigation, Meena et al. demonstrated that metakaolin and silica fume can improve the mechanical response of PP-fiber-reinforced mixtures; however, their analysis emphasized strength and first-crack deflection rather than a comprehensive evaluation of post-peak energy metrics or multivariable interactions among SCMs[20]. Even in broad review studies, such as Khan et al. the mechanical and durability-related contributions of SCMs in high-performance cementitious composites are discussed, yet detailed insights into post-cracking behavior, energy-based indices, and combined SCM effects in the presence of PP fibers remain largely unexplored[21].Accordingly, a clear research gap exists in the current literature: previous studies often investigate only one or two SCMs, report a limited set of performance indices, lack standardized terminal displacements for index extraction, and rarely provide multivariate analysis to quantify how binder components govern post-cracking behavior. To address this gap, the present study develops an extensive experimental program involving 44 HPFRCC mixtures incorporating simultaneous variations in cement, metakaolin, silica fume, slag, and limestone powder. Six key energy- and ductility-based indices are extracted from load–deflection curves using a uniform terminal displacement of 4 mm, and Spearman rank correlation analysis is applied to quantify the relative influence of each binder component on post-cracking performance. This integrated and data-driven approach constitutes the principal innovation of the study, offering a multidimensional understanding of how binder composition governs the flexural toughness and ductility of PP-fiber-reinforced HPFRCCs.

2. Materials and Methods

This study adopted an integrated experimental–analytical approach to investigate the mechanical behavior of

HPFRCCs. Multiple mixtures incorporating polypropylene fibers and various combinations of cement, metakaolin, silica fume, slag, and limestone powder were prepared to evaluate the influence of binder composition.Flexural performance was assessed through three-point bending tests following ASTM C1609. Load–displacement responses were then used to extract six key ductility and toughness indices using a consistent terminal displacement. Subsequently, Spearman's rank correlation analysis was applied to quantify the independent contribution of each binder component to post-cracking behavior. This methodology provided a systematic understanding of how binder variations govern energy absorption, ductility, and residual load capacity in PP-fiber-reinforced HPFRCCs.

2.1 Materials

All raw materials employed in this investigation were carefully selected based on their compatibility with high-performance cementitious composites and their conformity with relevant international standards (e.g., ASTM and EN specifications). Moreover, the initial ranges of mix design variables including cement, metakaolin, silica fume, ground granulated blast-furnace slag, limestone powder, water-to-binder ratio, and fiber volume fraction were determined in accordance with the guidelines and findings reported in previous experimental studies[22].This study employed HPFRCC mixtures incorporating pozzolanic supplementary cementitious materials and polypropylene fibers, following design principles established in prior experimental investigations to ensure realistic and mechanically viable mix proportions . Given the presence of five key mixture variables, a Taguchi L27 orthogonal array was adopted for the initial experimental screening a statistically efficient approach widely used in cementitious composite optimization to reduce the number of required trials while reliably identifying dominant factors[23]. The analysis indicated that cement, LP, MTK, and SL had the most significant effects on the post-cracking flexural behavior of HPFRCC, as shown in Figure 1.

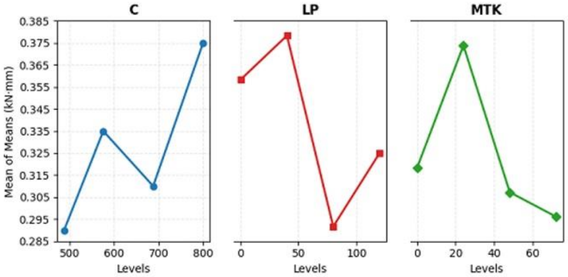

Fig. 1. Main effects of C, LP, MTK, on ductility obtained from Taguchi analysis.

The raw materials utilized in this research comprised Type I Portland cement, locally produced in Tehran, Iran, which met the requirements of ASTM C150[24].This cement served as the principal binding agent due to its consistent and reliable compressive strength development. The fine aggregate employed was naturally rounded, wind-deposited desert sand with a maximum particle size of 1.5 mm, conforming to ASTM C33 specifications and ensuring optimal particle packing within the matrix[25]. In addition, several supplementary cementitious materials (SCMs) were incorporated to enhance the matrix performance. Among these, silica fume (SF) with an average particle size of approximately 100 nm was used to improve pozzolanic reactivity and refine the microstructure.[26], finely ground limestone powder (LP, 1.5 µm) to improve packing density and alter hydration kinetics [27], Metakaolin (MTK, 1.5 µm), a highly reactive pozzolanic material, was incorporated to refine the pore structure and accelerate early strength development. In addition, ground granulated blast-furnace slag (SL, ≤ 1.5 mm) was used to improve the long-term durability and chemical stability of the composite matrix[28].Polypropylene fibers (PP) with a length of 12 mm, diameter of 19 µm, and tensile strength of 400 MPa were selected to improve the strain-hardening and crack-bridging capacity [29]Potable water complying with the requirements of ASTM C1602 was used in all mixtures to ensure consistency and chemical stability. Additionally, a polycarboxylate ether (PCE)-based superplasticizer was incorporated to achieve the desired workability and to promote uniform dispersion of fibers throughout the matrix.The raw materials utilized in this study, including silica fume, limestone powder (calcium carbonate), slag, and metakaolin, were characterized according to relevant ASTM standards prior to use, as illustrated in Figure 2.

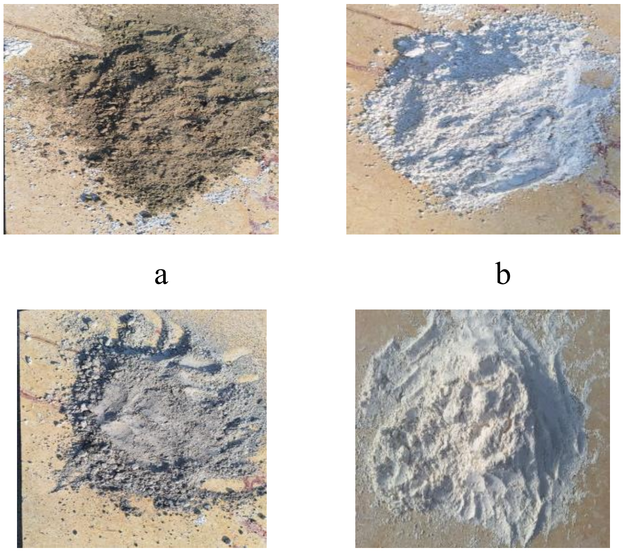

a b

c d

Fig. 2. Images of Raw Materials: (a) Silica Fume, (b) Calcium Carbonate Powder, (c) Slag, (d) metakaolin.

2.2 Mix Design and Specimen Preparation

To minimize the number of physical experiments while maintaining statistical reliability, the mix design optimization adopted the Taguchi orthogonal array approach, supported by prior experimental findings, particularly those reported by Feng et al. Considering the inclusion of five independent variables in the experimental program, a Taguchi L27 orthogonal array was employed to efficiently evaluate the parameter effects.[30]. This hybrid design approach enabled a systematic variation of key mix parameters including cement, supplementary cementitious materials (SCMs), and fiber content across a total of 44 mix formulations. All concrete specimens were produced and cured under controlled laboratory conditions in accordance with ASTM C192. The curing temperature was maintained at 20 ± 2 °C, and the relative humidity was kept above 90% throughout the process.A standardized pan-mixing procedure was employed to ensure uniformity in mixing time, rotation speed, and material loading sequence across all batches, thereby minimizing external variability. The procedure commenced with the dry blending of cement, SCMs (silica fume, slag, metakaolin, and limestone powder), and sand in a rotating drum mixer at 70 rpm for 60 s to achieve homogeneous distribution of dry ingredients. Subsequently, two-thirds of the total mixing water and superplasticizer were introduced, followed by mixing at 140 rpm for 120 s. Polypropylene (PP) fibers were gradually incorporated over a 10-minute period to prevent agglomeration and promote uniform dispersion. During fiber addition, the remaining water and superplasticizer were added in three incremental stages, each followed by mixing at 300 rpm for 30 s to maintain mixture homogeneity. The fresh HF-ECC was then cast into standard cube and beam molds and compacted using a vibrating table to eliminate air voids and ensure complete mold filling. After casting, all specimens were stored under ambient laboratory conditions for 24 hours, demolded, and subsequently water-cured for 28 days to ensure adequate hydration and strength development. Across all mixtures, the contents of polypropylene fibers (20 kg/m^3), sand (1128 kg/m^3), water (400 kg/m^3), and superplasticizer (12 kg/m^3) were kept constant to eliminate overlapping effects and ensure that variations in post-cracking behavior could be attributed solely to differences in binder composition. This approach is consistent with recent studies in which non-binder constituents are held constant to enable a clear and unbiased assessment of the influence of supplementary cementitious materials. Five binder components cement, metakaolin, silica fume, slag, and limestone powder were selected as variables because each contributes distinct mechanical and microstructural effects, including matrix densification, pore refinement, enhanced fiber matrix bonding, and modifications to post-peak response. Moreover, multi-component binder systems have become increasingly common in HPFRCC design, yet the independent and interactive effects of these SCMs, particularly in the presence of PP fibers, remain insufficiently explored. Therefore, selecting these five variables enables a more comprehensive and comparative evaluation of how binder composition governs energy- and ductility-related performance indices.[30].The first 28 mix designs are shown in Table 1.

Table 1: Mix Design Data a: N1–N28

Mix ID	SF	SL	MTK	Cement (C)	LP
N1	–	–	–	800	–
N2	–	–	24	736	40
N3	–	–	48	712	40
N4	–	–	72	688	40
N5	–	–	24	696	80
N6	–	–	48	672	80
N7	–	–	72	648	80
N8	–	–	24	656	120
N9	–	–	48	632	120
N10	–	–	72	608	120
N11	–	160	24	576	40
N12	–	120	48	552	40
N13	–	160	72	528	40
N14	–	160	24	536	80
N15	–	160	48	512	80
N16	–	160	72	488	80
N17	–	160	24	496	120
N18	–	160	48	472	120
N19	–	160	72	448	120
N20	–	80	24	656	40
N21	–	80	48	632	40
N22	–	80	72	608	40
N16	–	160	72	488	80
N17	–	160	24	496	120
N18	–	160	48	472	120
N19	–	160	72	448	120
N20	–	80	24	656	40
N21	–	80	48	632	40
N20	–	80	24	656	40
N21	–	80	48	632	40
N22	–	80	72	608	40
N23	–	80	24	616	80
N24	–	80	48	592	80
N25	–	80	72	568	80
N26	–	80	24	576	120
N27	–	80	48	552	120
N28	–	80	72	528	120

2.3 Mechanical Testing Procedures

A three-point bending test was performed to evaluate the flexural behavior and ductility of the HPFRCC specimens. All testing procedures were conducted in accordance with the relevant ASTM standards to ensure the reliability and reproducibility of the experimental results.

2.3.1 Flexural Test (Ductility Evaluation)

The flexural performance of the HPFRCC mixtures was evaluated through a three-point bending test conducted in accordance with ASTM C1609. Beam specimens with dimensions of 250 mm × 50 mm × 50 mm were prepared for each mix design and cured under water for 28 days prior to testing. The test setup consisted of two cylindrical supports spaced 180 mm apart, while a monotonic central load was applied using a servo-controlled actuator. The loading was performed at a constant displacement rate of 0.1 mm/s until specimen failure. For each mixture, three beam specimens were tested, and the average results were reported. Figure 3 illustrates the schematic arrangement of the three-point bending test and a representative crack pattern observed during flexural failure.

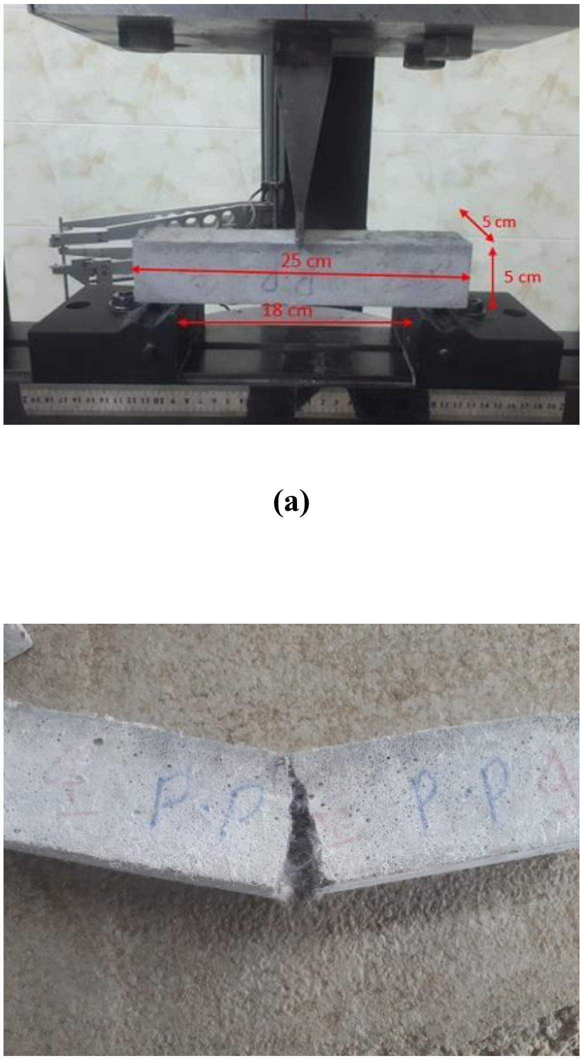

(a)

(b)

Fig. 3. a) Three-point bending test setup, and b) Crack pattern of the HPFRCC beam after flexural failure.

2.4 Analysis of the Load–Displacement Curve and Index Extraction

In the three-point bending test of HPFRCC specimens, the primary output of the testing apparatus was the load–displacement (P–Δ) curve, which illustrates the mechanical response of the specimen from the onset of loading to final failure. In this curve, the horizontal axis represents the mid-span displacement (Δ), while the vertical axis corresponds to the applied load (P).The general form of the P–Δ curve can be divided into three characteristic regions. The first is the ascending elastic branch, where the relationship between load and displacement is approximately linear. This is followed by a sudden load drop after the peak point, caused by matrix cracking and stiffness degradation. The final region is the gradual load recovery stage, resulting from the fiber-bridging mechanism, during which fibers bridge across cracks and restore part of the lost load-carrying capacity[31].The area under the load–displacement curve represents the mechanical work performed by the applied load during deformation. Since the load and displacement are expressed in kilonewtons (kN) and millimeters (mm), respectively, their product (kN·mm) corresponds to energy in joules (1 kN·mm = 1 J). Thus, the area enclosed by the P–Δ curve directly indicates the material's energy absorption capacity and ductility; a larger enclosed area signifies a tougher and more deformable material.In Figure 4, the load–displacement (P–Δ) response of five different specimens is presented. These specimens are identified by the codes N1, N4, N7, N16, and N32.

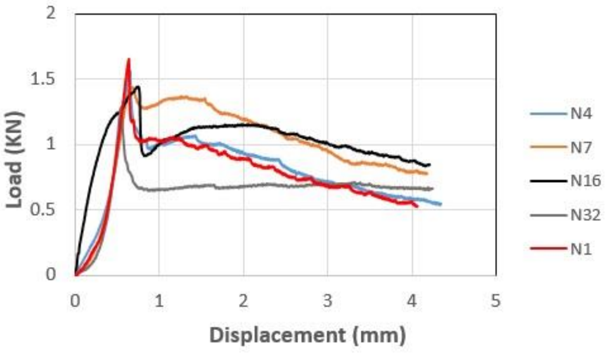

Fig. 4. Load–displacement curves of HPFRCC mixtures (N7, N4, N16, N32) showing different ductility levels.

For quantitative analysis, several characteristic points were identified from each load–displacement (P–Δ) curve, as schematically illustrated in Figure 5. The parameters Ppeak and Δpeak correspond to the maximum load and the associated displacement at the peak point, marking the end of the elastic stage. The parameters Pr and Δr denote the minimum load and displacement immediately following the sudden load drop, representing the onset of softening due to matrix cracking. Finally, Pu and Δu = 4 mm indicate the load and displacement at the fixed reference point used for comparative evaluation.

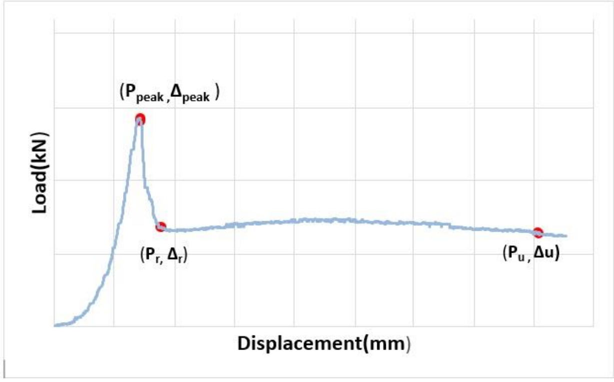

Fig. 5. Typical load–displacement (P–Δ) response of HPFRCC under three-point bending, showing the key characteristic points: peak load ($P_{□ea□}$, $\Delta_{□ea□}$), recovery point (P_r, Δ_r), and ultimate point (P_u, Δ_u).

The ultimate displacement of Δu = 4 mm was selected based on a sensitivity analysis of the load–displacement curves for all mixtures. The results indicated that beyond 4 mm, the post-peak responses tended to stabilize, and additional deformation contributed negligibly to the total absorbed energy. Adopting a constant terminal displacement ensured consistency in evaluating ductility and toughness indices and prevented variability caused by differences in post-peak softening behavior. This criterion is also consistent with previous HPFRCC studies, which commonly use fixed limits between 3 mm and 5 mm. Therefore, all indices in this study were computed using Δu = 4 mm as the standardized reference displacement.[32]. Table 2 summarizes the numerical data corresponding to the ten selected points identified on the load–displacement (P–Δ) curves. These values of load and displacement were directly obtained from the experimental measurements and form the basis for calculating the ductility and toughness indices discussed in the following section.

Table 2. Numerical data extracted from load–displacement (P–Δ) curves for selected HPFRCC mixtures.

N0	Δu (mm)	pu (kN)	Δr (mm)	pr (kN)	Δpeak (mm)	Ppeak (kN)
N1	4	0.85	0.95	1.05	0.65	1.6
N10	4	0.5	1.05	0.85	0.6	1.3
N18	4	0.75	0.9	1.1	0.6	1.75
N21	4	0.7	1.1	0.95	0.7	1.35
N22	4	0.65	1.05	0.85	0.65	1.25
N24	4	0.6	0.9	0.7	0.55	1.35
N26	4	0.5	0.8	0.6	0.5	1.1
N28	4	0.45	0.9	0.55	0.55	1.1

2.5 Formulation of Ductility and Failure Indices

To quantitatively assess the post-cracking behavior and energy absorption capacity of the high-performance fiber-reinforced cementitious composites (HPFRCCs), a series of mechanical indices were developed based on the experimental load–displacement (P–Δ) responses. These indices were designed to capture various aspects of flexural performance, including elastic stiffness, energy dissipation, post-peak recovery, and residual strength.

Across all experimental curves, four characteristic stages were consistently identified. The yield stage corresponds to the termination of the linear elastic region, where microcracks initiate and deviation from linearity begins. The peak stage represents the point at which the maximum load is reached, typically prior to the formation of a major crack. The recovery stage is characterized by a partial restoration of load capacity, attributed to the fiber-bridging mechanism following the initial post-peak drop. Finally, the ultimate stage is defined at a displacement of 4 mm, where the post-peak softening response becomes nearly stable across all mixtures.

These stages serve as reference boundaries for evaluating the ductility, toughness, and integrity indices. The choice of the ultimate displacement value was determined through the previously discussed sensitivity analysis, ensuring that all specimens were assessed within a consistent deformation domain. This standardized criterion minimizes variability associated with differences in failure progression and enables reliable comparison among all HPFRCC mixtures.

2.5.1 EnergyBased Ductility Index (μ_E)

The energy-based ductility index provides a physically meaningful measure of the material's ability to undergo inelastic deformation after cracking.

Unlike conventional displacement ratios, this index quantifies the mechanical work performed by the load during both the elastic and post-peak phases, allowing a more reliable comparison among mixtures exhibiting different softening behaviors.

In this approach, the elastic portion of the load–displacement curve represents the energy stored prior to cracking, while the post-peak region reflects the energy absorbed through fiber bridging, matrix deformation, and crack opening.

The ratio of these two energy components defines the ductility index, where a higher value indicates greater deformation tolerance and energy dissipation capacity of the composite[33].

$$\mu_E = \frac{E_{elastic}}{E_{post}} = \frac{P_{peak} \cdot \Delta_{peak}}{\left(P_{peak} + P_U\right) \cdot \left(\Delta_u - \Delta_{peak}\right)} \qquad (1)$$

The term Eelastic represents the strain energy stored within the specimen during the elastic phase, that is, before the maximum load is reached.

The parameter *Epost* corresponds to the energy absorbed during the post-peak softening stage, when deformation continues under decreasing load due to fiber bridging and matrix cracking. Ppeak denotes the highest load sustained by the specimen during flexural testing, while *Pu* indicates the residual load recorded at the terminal displacement. The displacements Δpeak and Δu correspond to the deformation at the peak load and at the fixed limit of four millimeters, respectively.

Both energy terms, *Eelastic* and *Epost*, are expressed in kilonewton–millimeters (kN·mm) , a unit directly equivalent to joules (1 kN·mm = 1 J). This ensures that the calculated ductility index reflects a consistent and physically interpretable measure of mechanical energy absorption and deformation capacity among all mixtures.

2.5.2 Failure Work Index (FWI)

The Failure Work Index represents the total mechanical energy absorbed by the specimen during flexural loading up to the terminal displacement of four millimeters. It is defined as the area under the entire load–displacement curve and can be expressed as:

$$FWI = \int_0^{\Delta_u} P(\Delta) \cdot d\Delta \qquad (2)$$

where P(Δ) is the applied load at displacement Δ.

In this study, the value of FWI was computed numerically using the trapezoidal rule. Higher values of this index indicate greater overall toughness and energy dissipation capacity, reflecting the ability of the composite to sustain deformation and resist brittle failure[34].

2.5.3 Softening Ductility Ratio (SDR)

The Softening Ductility Ratio quantifies the ability of the composite to retain load-carrying capacity after the peak point, reflecting the contribution of fibers to post-cracking resistance. It is defined as the ratio of the residual load at the terminal displacement to the maximum load sustained by the specimen:

$$SDR = \frac{P_u}{P_{peak}} \qquad (3)$$

where Pu is the load at the ultimate displacement (4 mm) and *Ppeak* is the peak load. A higher SDR indicates a more stable post-peak response and better fiber bridging performance, signifying enhanced ductility and toughness of the composite[35].

2.5.4 Recovery Index (RI)

The Recovery Index evaluates the degree of load recovery after the initial post-peak drop, representing the fiber-bridging efficiency and the composite's self-restoring capability. It is defined as the ratio of the recovered load after the minimum point to the difference between the peak and minimum loads:

$$RI = \frac{(P_r - P_u)}{(P_{peak} - P_u)} \qquad (4)$$

where Ppeak is the maximum load, *Pr* is the recovered load after the initial drop, and *Pu* is the residual load at the ultimate displacement. A higher RI denotes a greater capacity of the fibers to recover and redistribute stresses after cracking[36].

2.5.5 Residual Toughness Factor (RTF)

The Residual Toughness Factor quantifies the relative contribution of the post-peak region to the total absorbed energy, providing an integrated measure of the material's toughness beyond cracking. It is defined as the ratio of the post-peak energy to the total energy absorbed up to the terminal displacement:

$$RTF = \frac{E_{post}}{\left(E_{elastic} + E_{post}\right)} \qquad (5)$$

where Epost is the energy absorbed after the peak load and Eelastic is the energy accumulated before the peak.

This factor expresses the percentage of energy dissipation that occurs during the softening phase.

Higher RTF values indicate improved energy absorption and greater ductility of the HPFRCC under flexural loading[37].

2.5.6 Toughness Modulus (TM)

The Toughness Modulus expresses the energy absorption capacity per unit volume of the specimen, linking the mechanical energy absorbed during flexural deformation to the specimen geometry. It is calculated by normalizing the total absorbed energy (Failure Work Index) with respect to the specimen's volume subjected to bending:

$$TM = \frac{FWI}{V} \qquad (6)$$

where FWI is the total absorbed energy (in kN·mm or J) and *V* is the effective volume of the prism under bending (in mm^3). This normalization allows for a geometry-independent comparison among different mixtures or testing setups.

A higher TM value indicates superior energy absorption efficiency and improved structural performance per unit material volume[37].

2.6 Sensitivity Analysis Using Spearman Correlation

To quantitatively examine the influence of input material parameters on the ductility and toughness indices, a non-parametric correlation analysis was performed using the Spearman's rank correlation coefficient (ρ). This method evaluates the monotonic relationship between two variables without assuming linearity or normal distribution, making it particularly suitable for datasets with limited sample size or nonlinear dependencies common in experimental HPFRCC studies[38].

The Spearman coefficient (ρ) is computed as:

$$\rho = 1 - \frac{6\sum {d_i}^2}{n(n^2 - 1)} \qquad (7)$$

where d_i represents the difference between the ranked values of the input and output variables, and n is the number of data pairs. The value of ρ ranges between -1 and $+1$, where positive values indicate a direct (increasing) relationship and negative values represent an inverse (decreasing) trend.

In this study, the input variables included C, LP, MTK, SF, and SL, while the output indices were μE, SDR, FWI, RI, RTF, and TM. All variables were normalized prior to computation to ensure comparable scaling. The results were visualized using a color-coded heatmap, where warm colors represent positive correlations and cool colors indicate negative relationships.

To avoid misinterpretation, it should be noted that the Spearman correlation analysis applied in this study evaluates independent monotonic relationships between individual binder components and mechanical indices; therefore, potential interaction effects among SCMs (such as cement–slag synergy or metakaolin–silica fume overlap) were not explicitly assessed and remain outside the scope of this investigation.

3. Results and Discussion

3.1 Overview

This section presents and interprets the key experimental results, focusing on the flexural response of HPFRCC mixtures as represented by their load–displacement (P–Δ) behavior. A total of 44 mix designs were evaluated under three-point bending tests, and six energy-based indices μE, FWI, SDR, RI, RTF, and TM were systematically derived from the experimental curves. The analysis addresses four main aspects: (i) the interrelation between ductility indicators such as μE and SDR, (ii) the comparative performance of top mixtures in terms of toughness and residual strength, (iii) a comprehensive ranking of all mixtures based on their overall post-cracking behavior, and (iv) the sensitivity of these indices to variations in mix composition using Spearman's correlation. Collectively, the results establish an experimentally validated, physics-based framework that elucidates how binder composition governs the ductility and toughness characteristics of PP-fiber-reinforced HPFRCCs.

3.2 Interrelation of Ductility Indicators μ_E and SDR

The relationship between μE and SDR is presented in Figure 6. Each data point corresponds to one HPFRCC mixture, with the color gradient representing E_total in kN·mm. A moderately positive trend can be observed between μE and SDR, suggesting that mixtures exhibiting greater post-peak stiffness retention tend to possess higher ductility. Nevertheless, noticeable data scatter is evident, highlighting the nonlinear and composition-dependent nature of post-cracking behavior influenced by fiber–matrix interaction.

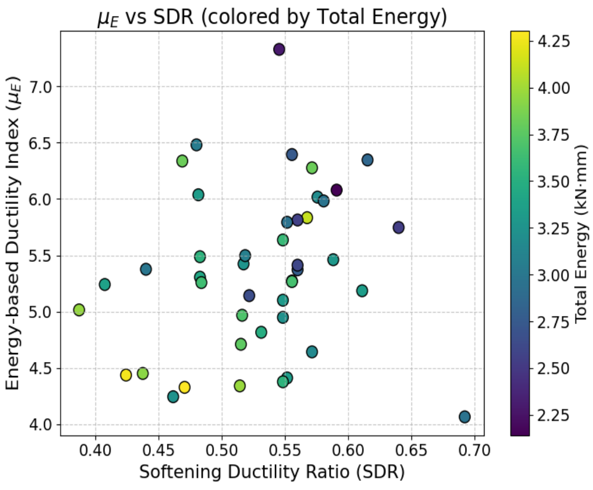

Fig. 6. Correlation between μE and SDR for all HPFRCC mixtures, with the color scale representing total absorbed energy (E_total).

3.3 Evaluation of TM, RI, and RTF Indices in High-Performance Mixtures

To compare the post-cracking performance of the mixtures, three representative indices TM, RI, and RTF were evaluated for the top five mixes, as shown in Figure 7. These mixtures (N26, N22, N1, N7, and N4) were selected for their superior energy absorption, post-peak stability, and residual capacity. Among them, N26 exhibited the highest TM value, indicating the greatest energy absorption capability prior to failure, while maintaining balanced performance in RI and RTF.

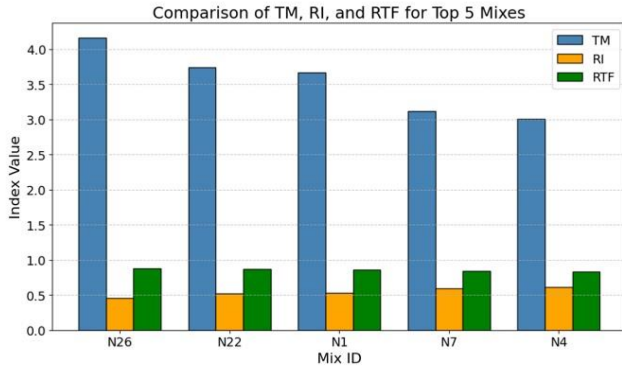

Fig. 7. Comparison of TM, RI, and RTF values for the top five HPFRCC mixtures.

3.4 Summary of Results

Table 3 presents the ten mixes with the highest overall performance based on μE, FWI, RI, R_SD, RTF, and TM. Mix N26 achieved the top rank, demonstrating excellent energy absorption capacity (high μE and TM) and well-balanced residual behavior with an RI value around 0.45. Mixes N22 and N1 followed closely, showing consistent and reliable performance across all evaluated indices. In comparison, mixes N28 and N33 displayed slightly lower toughness (TM) but maintained stable post-peak recovery, with RTF values close to 0.86.

Table 3. Top 10 HPFRCC Mixes Ranked by Overall Mechanical Performance

Mix ID	μE	FWI (kN·mm)	RI	R_SD	RTF	TM
N1	6.34	3.82	0.53	0.47	0.86	3.67
N10	6.35	2.87	0.38	0.62	0.86	3.67
N18	6.28	3.82	0.43	0.57	0.86	3.64
N21	6.04	3.33	0.52	0.48	0.86	3.52
N22	6.48	3.04	0.52	0.48	0.87	3.74
N24	6.39	2.75	0.44	0.56	0.86	3.70
N26	7.33	2.29	0.45	0.55	0.88	4.16
N28	6.08	2.14	0.41	0.59	0.86	3.54

3.5 Sensitivity of Ductility Indices to Mix Proportions

To evaluate the influence of mix composition on mechanical behavior, Spearman correlation coefficients (ρ) were computed between each ductility-related index and the primary mix parameters. The results, presented in Figure 8, illustrate both the magnitude and direction of correlations between the material constituents and the mechanical performance indices.

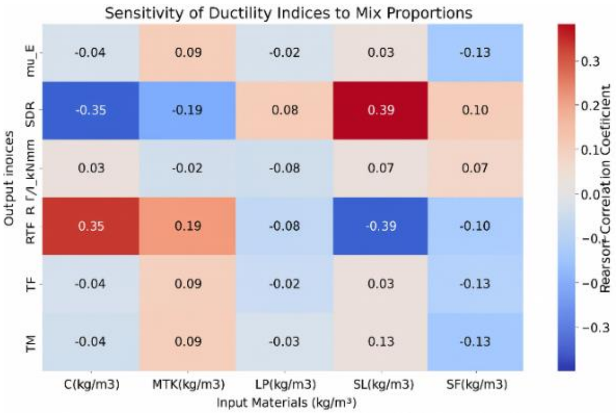

Fig. 8. Sensitivity of ductility and toughness indices to mix proportions, based on Spearman's rank correlation coefficients.

3.6 Discussion

3.6.1 Discussion on µE–SDR Relationship

The results reveal that the ductility behavior of HPFRCC mixtures cannot be described by a single parameter.Although µE and SDR both represent aspects of post-cracking deformability, their correlation is onlypartial. Mixtures with higher SDR valuesindicating slower stiffness degradation tend to exhibit enhanced µE, confirming that improved energy dissipation is linked to stable post-peak response.Nevertheless, the data dispersion implies that other factors such as fiber dispersion, matrix rheology, and interfacial bond strength also play crucial roles in determining ductility.The color mapping of total energy further emphasizes that the highest µE values correspond to intermediate SDR levels, suggesting an optimum balance between stiffness reduction and energy absorption.This finding aligns with previous HPFRCC studies, where excessive softening (low SDR) or overly stiff matrices (high SDR) both resulted in suboptimal ductility performance.

3.6.2 iscussion on TM, RI, and RTF Indices

The comparison reveals that higher TM values do not necessarily coincide with higher RI or RTF values, suggesting that total toughness and residual stability do not always peak simultaneously.

Mix N26, which recorded the highest TM, demonstrates the greatest overall energy absorption capacity, whereas Mixes N7 and N4 exhibited relatively higher RI values, implying better post-peak load retention and enhanced crack-bridging effectiveness. These variations are primarily attributed to differences in mix composition and fiber dispersion, which influence the fiber–matrix interfacial bonding and consequently the residual stress transfer capability. Overall, Mixes N26 and N22 showed the most favorable post-cracking behavior, characterized by a balanced combination of toughness, ductility, and residual strengthfindings consistent with the previously discussed µE and SDR trends.

3.6.3 Discussion on Comprehensive Performance Ranking

The comprehensive ranking highlights that optimal HPFRCC performance is achieved through a balanced synergy between ductility and residual stability rather than maximization of a single parameter. Mix N26, with the highest µE and TM, represents the most energy-efficient composite, maintaining both high deformation capacity and moderate post-peak load retention. Mixes N22 and N1, which follow closely, exhibit well-proportioned RI and RTF values, signifying stable post-cracking stress transfer supported by effective fiber–matrix interaction.

By contrast, mixtures like N33 and N28 achieved slightly lower µE values due to faster stiffness degradation (higher RSD), but their overall performance remained competitive because of adequate residual toughness.Overall, this ranking confirms that mixtures with optimized cement content, moderate limestone powder, and balanced superplasticizer dosage tend to yield superior ductility–toughness synergy.

These findings are consistent with previous studies emphasizing that energy-based evaluation provides a more comprehensive criterion for assessing HPFRCC behavior than conventional strength-based parameters alone.

3.6.4 Interpretation of Spearman Correlation Results

The Spearman correlation analysis demonstrated that C had a positive association with RI, implying improved residual load capacity at higher cement content. In contrast, SL exhibited a negative correlation with both RI and SDR, indicating that excessive fluidity reduces fiber–matrix interaction and accelerates stiffness degradation. The influence of MTK was generally moderate and positive across most indices, suggesting improved microstructure and delayed cracking. SF showed almost negligible correlations, indicating that its effect on ductility becomes saturated beyond an optimum level. LP exhibited weakly negative trends, confirming its minor dilution effect when replacing part of the cement. Among all output indices, SDR was found to be the most sensitive to variations in mix proportions, particularly SL and C, demonstrating its suitability as a key indicator of post-cracking deformation behavior.

Overall, these results confirm that ductility and toughness in HPFRCCs are controlled by a balanced combination of matrix composition, packing density, and fiber–matrix bond performance.

3.6.5 Comparison with Previous Studies

The findings of this study are generally consistent with previous works that have examined the effects of PP fibers on post-cracking ductility and energy absorption. The results confirm that higher binder content and a well-balanced mix composition lead to improvements in μE, TM, and RI, aligning with the trends observed in prior FRCC and HPFRCC studies emphasizing stable fiber–matrix interaction and controlled crack propagation. However, the range of index values obtained in this study is broader, revealing that mixtures with higher SL content, while retaining reasonable residual strength, tend to exhibit weaker post-peak stability and reduced toughness an aspect less emphasized in earlier reports. Overall, whereas most previous studies have focused on the isolated influence of fibers or one or two supplementary materials, the present work demonstrates that the combined interaction of all binder components (C, MTK, SL, SF, and LP) plays a decisive role in simultaneously optimizing ductility, post-peak stiffness, and energy absorption in HPFRCC mixtures.[9,15–17]

3.6.6 Limitations and Future Work

This study, while establishing a comprehensive framework for ductility and toughness indices, faced limitations primarily related to its experimental dataset size (44 mixtures), which may affect the statistical robustness and generalizability of the derived correlations. The absence of resampling techniques like k-fold cross-validation also limits a rigorous assessment of model stability.

Future research should focus on expanding the experimental database to include a wider range of mix proportions and material types. Furthermore, microstructural investigations (e.g., using SEM) are essential to link the observed mechanical performance to underlying mechanisms such as fiber dispersion and fiber-matrix interface. Finally, broader validation of these indices across various HPFRCC types and loading conditions is recommended to confirm their universal applicability.

4 . Conclusion

This study shows that evaluating the post-cracking behavior of PP-reinforced HPFRCCs requires a multidimensional approach based on the P–Δ response rather than strength-based criteria alone. Using six energy-related indices (μE, FWI, SDR, RI, RTF, and TM) extracted at a fixed terminal displacement of 4 mm enabled consistent comparison across all mixtures. The results indicate that mixtures containing higher proportions of cement and MTK achieved the best post-cracking performance, characterized by greater energy absorption, improved post-peak stability, and higher residual load capacity. These mixtures exhibited a denser matrix and more effective fiber–matrix interaction, leading to a more stable softening response. In contrast, mixtures with increased SL content showed reduced SDR and RTF values, reflecting weaker post-peak stability. SF primarily enhanced matrix densification but did not independently produce the highest ductility levels. Overall, mixtures optimized with cement–MTK–LP combinations and limited SL content demonstrated the highest mechanical efficiency in terms of energy absorption and controlled softening. These findings suggest that the design of HPFRCCs for seismic and dynamic applications should prioritize ductility, energy dissipation, and residual capacity rather than relying solely on peak strength, as these attributes are essential for structural resilience and collapse prevention.

Novelty of the Study:

- This study introduces a multidimensional, energy-based approach that provides a more accurate assessment of post-cracking behavior compared to traditional strength-based criteria.
- The results demonstrate that optimized combinations of cement, metakaolin, and limestone powder significantly improve energy absorption, post-peak stability, and residual load capacity.
- A correlation-driven analytical framework is employed to distinguish the individual influence of each binder component and identify mix designs with superior mechanical efficiency.

5.Ethical Approval:

Material Availability Statement: All materials used in this study were commercially sourced and characterized in accordance with international standards prior to use. Full sourcing details are provided in Section 2.1 of this paper.

Statements and Declarations

Competing Interests and Funding:

The authors declare that they have no known competing financial interests or personal relationships that could have appeared to influence the work reported in this paper.

Data availability:

All data generated or analyzed during this study are included in this published article.

References

[1]. I. da Silva Brito, D. Alan Strauss Rambo, S. Martini, R. Pícolo Salvador, M. Fabrízio de Menezes Freitas, Flexural behavior of HPFRCC: Enhancing post-crack strength and toughness by magnetic alignment of the reinforcement, Constr Build Mater 269 (2021) 121265. https://doi.org/10.1016/j.conbuildmat.2020.121265.

[2]. Z. Feng, C. Li, D.-Y. Yoo, R. Pan, J. He, L. Ke, Flexural and cracking behaviors of reinforced UHPC beams with various reinforcement ratios and fiber contents, Eng Struct 248 (2021) 113266. https://doi.org/10.1016/j.engstruct.2021.113266.

[3]. A. V. Lopes, T. Lou, S.M.R. Lopes, On the ductility of RC beam section: A revision and up to date of conclusions, Eng Struct 322 (2025) 119105. https://doi.org/10.1016/j.engstruct.2024.119105.

[4]. J.H. Ling, Y.T. Lim, E. Jusli, Methods to Determine Ductility of Structural Members: A Review, Journal of the Civil Engineering Forum (2023) 181–194. https://doi.org/10.22146/jcef.6631.

[5]. D.-Y. Yoo, S. Kim, G.-J. Park, J.-J. Park, Residual performance of HPFRCC exposed to fire – Effects of matrix strength, synthetic fiber, and fire duration, Constr Build Mater 241 (2020) 118038. https://doi.org/10.1016/j.conbuildmat.2020.118038.

[6]. S. Xun, Y. Shiping, Y. Yuhou, F. Jian, L. Litao, Comparative analysis of flexural performance of old full-scale hollow slab beams reinforced with fiber composites, Constr Build Mater 338 (2022) 127657. https://doi.org/10.1016/j.conbuildmat.2022.127657.

[7]. M.R. Mahmoud, X. Wang, B. Xingyu, M. Altayeb, S. Liu, A.M. Moussa, Flexural behaviour of semi-precast slabs of fibre-reinforced concrete reinforced with prestressed basalt fibre-reinforced polymer and steel bars, Advances in Structural Engineering 27 (2024) 2609–2625. https://doi.org/10.1177/13694332241276059.

[8]. C. Tian, Z. Zheng, X. Wei, A new fracture toughness calculation method for cementitious materials in the three-point bending test based on the transverse force, Case Studies in Construction Materials 17 (2022) e01215. https://doi.org/10.1016/j.cscm.2022.e01215.

[9]. H. Chen, H. Wang, J. Zheng, Z. Wu, Residual fracture toughness and fracture energy of concrete with different strengths after fatigue loading, Constr Build Mater 408 (2023) 133563. https://doi.org/10.1016/j.conbuildmat.2023.133563.

[10]. W. Chen, C. Zheng, C. Jia, B. Hu, D. Li, Strain-rate dependence of the dynamic softening in a duplex stainless steel, Mater Charact 162 (2020) 110219. https://doi.org/10.1016/j.matchar.2020.110219.

[11]. S. Park, S. Wu, Z. Liu, S. Pyo, The Role of Supplementary Cementitious Materials (SCMs) in Ultra High Performance Concrete (UHPC): A Review, Materials 14 (2021) 1472. https://doi.org/10.3390/ma14061472.

[12]. M.R. Latifi, Ö. Biricik, A. Mardani Aghabaglou, Effect of the addition of polypropylene fiber on concrete properties, J Adhes Sci Technol 36 (2022) 345–369. https://doi.org/10.1080/01694243.2021.1922221.

[13]. Z.F. Akbulut, E. Kuzielová, T.A. Tawfik, P. Smarzewski, S. Guler, Synergistic Effects of Polypropylene Fibers and Silica Fume on Structural Lightweight Concrete: Analysis of Workability, Thermal Conductivity, and Strength Properties, Materials 17 (2024) 5042. https://doi.org/10.3390/ma17205042.

[14]. M.M.A. Elahi, C.R. Shearer, A. Naser Rashid Reza, A.K. Saha, M.N.N. Khan, M.M. Hossain, P.K. Sarker, Improving the sulfate attack resistance of concrete by using supplementary cementitious materials (SCMs): A review, Constr Build Mater 281 (2021) 122628. https://doi.org/10.1016/j.conbuildmat.2021.122628.

[15]. P. Smarzewski, Comparative Fracture Properties of Four Fibre Reinforced High Performance Cementitious Composites, Materials 13 (2020) 2612. https://doi.org/10.3390/ma13112612.

[16]. A.A. Del Savio, D. La Torre Esquivel, J.M. García Landeo, Post-Cracking Properties of Concrete Reinforced with Polypropylene Fibers through the Barcelona Test, Polymers (Basel) 15 (2023) 3718. https://doi.org/10.3390/polym15183718.

[17]. M. Garg, P. Azarsa, R. Gupta, Self-Healing Potential and Post-Cracking Tensile Behavior of Polypropylene Fiber-Reinforced Cementitious Composites, Journal of Composites Science 5 (2021) 122. https://doi.org/10.3390/jcs5050122.

[18]. P. Smarzewski, A. Jancy, Comparative Study on Mechanical Performance and Toughness of High-Performance Self-Compacting Concrete with Polypropylene and Basalt Fibres, Materials 18 (2025) 3833. https://doi.org/10.3390/ma18163833.

[19]. B. Wei, X. He, W. Wu, C. Wu, J. He, Research on the flexural behavior of polypropylene fiber reinforced concrete beams with hybrid reinforcement of GFRP and steel bars, Mater Struct 57 (2024) 66. https://doi.org/10.1617/s11527-024-02343-9.

[20]. Effect of metakaolin and silica fume with polypropylene fiber on the properties of concrete pavement incorporating taguchi analysis, Indian Journal of Engineering and Materials Sciences 32 (2025). https://doi.org/10.56042/ijems.v32i01.12220.

[21]. R.J. Thomas, S. Peethamparan, Stepwise regression modeling for compressive strength of alkali-activated concrete, Constr Build Mater 141 (2017) 315–324. https://doi.org/10.1016/j.conbuildmat.2017.03.006.

[22]. M. Alameri, M.S.M. Ali, M. Elchalakani, A. Sheikh, Optimizing slag-based geopolymer mix design for enhanced strength and durability, Journal of Building Engineering 100 (2025) 111770. https://doi.org/10.1016/j.jobe.2025.111770.

[23]. S. Khrais, A. Mohammed, A.A. Al, T. Darabseh, Effect of TIG welding parameters on 316 L stainless steel joints using taguchi L27 approach, Mater Res Express 11 (2024) 016512. https://doi.org/10.1088/2053-1591/ad1cab.

[24]. D.W. Dunker, J. Farny, Your Pipe Lining Has a New Cement—ASTM C150 Compared to ASTM C595, in: Pipelines 2024, American Society of Civil Engineers, Reston, VA, 2024: pp. 312–320. https://doi.org/10.1061/9780784485569.034.

[25]. H. Cabrera, C. Daza, C. Pacheco-Bustos, M. Murillo, Study on mechanical properties of mortars containing steel shot and sea sand as fine aggregate replacement, IOP Conf Ser Mater Sci Eng 1126 (2021) 012003. https://doi.org/10.1088/1757-899X/1126/1/012003.

[26]. E. Wang, L. Xiang, B. Tang, X. Dai, Z. Cao, T. Jiang, Y. Wang, X. Chen, W. Li, Y. Zhao, K. Yang, X. Wu, Preparation and Compression Resistance of Lightweight Concrete Filled with Lightweight Calcium Carbonate Reinforced Expanded Polystyrene Foam, Polymers (Basel) 15 (2023). https://doi.org/10.3390/polym15244642.

[27]. L. Dvorkin, V. Zhitkovsky, S. Lapovskaya, Y. Ribakov, Investigation of the Cementing Efficiency of Fly Ash Activated by Microsilica in Low-Cement Concrete, Materials 16 (2023). https://doi.org/10.3390/ma16216859.

[28]. T. Wang, H. Han, Y. Wang, A two-stage distributionally robust optimization model for geothermal-hydrogen integrated energy system operation considering multiple uncertainties, Environ Dev Sustain 24 (2023) 132–144. https://doi.org/10.1007/s10668-023-03294-x.

[29]. B. Sadowska-Buraczewska, M. Szafraniec, D. Barnat-Hunek, G. Lagód, Flexural behavior of composite concrete slabs made with steel and polypropylene fibers reinforced concrete in the compression zone, Materials 13 (2020). https://doi.org/10.3390/MA13163616.

[30]. Z. Feng, Y. Zhou, L. Sui, Z. Zhu, Optimal design of a low-cost high-performance hybrid fiber engineered cementitious composites, Constr Build Mater 345 (2022). https://doi.org/10.1016/j.conbuildmat.2022.128372.

[31]. W. Guo, P. Zhang, Y. Tian, B. Wang, W. Ma, Influence of the Amount of Steel Fibers on Fracture Energy and Drying Shrinkage of HPFRCC, Advances in Materials Science and Engineering 2020 (2020). https://doi.org/10.1155/2020/8459145.

[32]. Y. Shao, S.L. Billington, Impact of cyclic loading on longitudinally-reinforced UHPC flexural members with different fiber volumes and reinforcing ratios, Eng Struct 241 (2021) 112454. https://doi.org/10.1016/j.engstruct.2021.112454.

[33]. H.-B. Lin, Calculation of Ultimate Ductility Index Based on Hysteretic Energy Analysis of the Restoring Force Curve, Buildings 15 (2025) 3152. https://doi.org/10.3390/buildings15173152.

[34]. S. Chen, P. Jain, E. Ramsey, J. Chen, M. Flannigan, Comparative Analysis of Ensemble and Deterministic Models for Fire Weather Index (FWI) System Forecasting, Weather Forecast (2025). https://doi.org/10.1175/WAF-D-25-0069.1.

[35]. S. Wang, W. Wang, D.G. Lignos, Uniaxial material model with softening for simulating the cyclic behavior of steel tubes in concrete□filled steel tube beam□columns, Earthq Eng Struct Dyn 53 (2024) 4032–4053
.https://doi.org/10.1002/eqe.4204.

[36]. S. Bhattacharyya, B.D. Sarkar, S. Sarkar, P.K. Singh, R. Manatkar, Developing a reintegration index (RI) for a closed-loop supply chain network in the automobile industry, Benchmarking: An International Journal (2025). https://doi.org/10.1108/BIJ-05-2024-0375.

[37]. C. Liu, J. Sun, C. Wang, F. Li, T. Hussain, Fracture behaviour, microstructure, and performance of various layered-structured Al2O3-TiC-WC-Co composites, Ceram Int 47 (2021) 19766–19773. https://doi.org/10.1016/j.ceramint.2021.03.315.

[38]. E.F. El-Hashash, R.H.A. Shiekh, A Comparison of the Pearson, Spearman Rank and Kendall Tau Correlation Coefficients Using Quantitative Variables, Asian Journal of Probability and Statistics (2022) 36–48. https://doi.org/10.9734/ajpas/2022/v20i3425